UMYU Scientifica, Vol. 4 NO. 1, March 2025, Pp 297 – 304
https://doi.org/10.56919/usci.2541.029
ISSN: 2955 – 1145 (print); 2955 – 1153 (online)
A periodical of the Faculty of Natural and Applied Sciences, UMYU, Katsina

ORIGINAL RESEARCH ARTICLE

DFT Investigation of Magnesium-Doped Zirconolite for High-Level Nuclear Waste Immobilization

Yahaya Aliyu[1]*, Abubakar Yahaya Kauru[2], Abdullahi Lawal[1], Alhassan Shuaibu[3], and Yusuf Musa Abubakar[4]

[1]Department of Physics, Faculty of Physical Sciences, Ahmadu Bello University, Zaria, Nigeria
[2]Ground Studies Department, Flying School, Nigerian College of Aviation Technology, Zaria Aerodrome, Kaduna, Nigeria
[3]Department of Physics, Kaduna State University, Kaduna, Nigeria
[4]Centre for Energy Research and Training, Ahmadu Bello University, Zaria, Nigeria

ABSTRACT

The black mineral zirconolite ($CaZrTi_2O_7$), which is made up of calcium zirconium titanate, has been considered an appropriate waste form for immobilizing radioactive waste. Using Density Functional Theory (DFT), this study examined the impact of magnesium substitution on ceramic nuclear waste from Zirconolite. To explore the material's structural stability and electronic characteristics, a computational simulation was conducted using Quantum ESPRESSO within the Perdew-Burke-Ernzerhof generalized gradient approximation (PBE-GGA) and Broyden-Fletcher-Golfarb-Shannon (BFGS) relaxation calculations. From the energy range of -2.0 eV to 2.0 eV, the computed electronic band structure was displayed along the symmetry routes. An indirect band gap material with 0.06 eV was revealed by the energy gap between the valence band maximum (VBm) and the conduction band minimum (CBm) at the R2 and Γ sites. The behavior of semiconductors is consistent with this energy gap value. The dopant substitution energy effect was determined to be 1.424 eV, indicating that the Mg-doped Zirconolite's molecular structure remained stable. To sum up, doping $CaZrTi_2O_7$ ceramic may promote the production of oxygen, which enhances Magnesium's mobility to the subterranean water molecules inside the geological disposal facility.

ARTICLE HISTORY

Received December 25, 2024
Accepted March 28, 2025
Published March 31, 2025

KEYWORDS

DFT; Mg-doped, Zirconolite; High-Level-Waste; Structural and electronic properties

INTRODUCTION

The world is currently facing serious issues relating to greenhouse gas emissions (GHGs) caused by global warming due to energy production (Musa et al., 2022) (Aliyu et al., 2024). The production of clean energy is crucial to support the everyday life of human beings and to drive economic growth and development. Recently, to meet the requirements of clean energy generation, nuclear energy has become a preferable option and has been broadly investigated due to its high energy density, low-cost, and absence of air pollution (Hurley et al., 2022; Mathew, 2022). While we cannot completely rely on renewable energy sources, the applications of nuclear reactors as a major energy source can secure the disposition of spent nuclear fuel, and this can ultimately represent the future of clean energy (Pastina *and* Laverne, 2021). Radionuclides are finding increasing applications in the fields of medicine, chemical industry, and agriculture but produce radioactive waste materials in the process. In terms of the production and operation of the nuclear fuel cycle, radioactive waste by-products generated are potentially harmful (Subba Rao *et al.*, 2022).

High-level radioactive waste (HLW) as a nuclear power plant's by-product has threatened the public and the environment (Ma *et al.*, 2018). The current solutions include reprocessing through *mixed oxide* (MOX), fuel conversion, and immobilization by direct disposal in the Geological Disposal Facility (GDF) (Schreinemachers *et al.*, 2022; Tanti *and* Kaltsoyannis, 2021). Among the different solutions, immobilization is crucial to mitigate this issue. Immobilization refers to waste transformation by atomistic replacement of radioisotopes inside a waste form. Nuclear waste substances provide different conditions comprising long-term stability, leaching endurance, and high waste stacking. Based on the category of the waste to be incorporated, a waste form must provide chemical flexibility to incorporate many radionuclides and impurities as well as a high tolerance

Correspondence: Yahaya Aliyu. Department of Physics, Faculty of Physical Sciences, Ahmadu Bello University, Zaria, Nigeria. ✉ yadabo@abu.edu.ng.
How to cite: Aliyu, Y., Kauru, Y. A., Lawal, A., Shuaibu, A., & Abubakar, Y. M. (2025). DFT Investigation of Magnesium-Doped Zirconolite for High-Level Nuclear Waste Immobilization. *UMYU Scientifica*, 4(1), 297 – 304. https://doi.org/10.56919/usci.2541.029

against radiation damage (Neumeier *et al.,* 2017). For instance, borosilicate glasses have been used as an HLW immobilization matrix globally, and exciting results have been achieved (Jafar *et al.,* 2021). However, minor actinides, less solubility, lower activity loading, and devitrification are the limitations of glass matrices. Synroc is proposed as an analogue titanate mineral that can replace borosilicate glasses for HLW immobilization. Synroc entails zirconolites, perovskites, hollandites, pyrochlore and rutile type phases. Zirconolite is a naturally occurring titanate ceramic and the main holding phase for actinides among synroc ceramic waste forms (Blackburn et al., 2020; Blackburn et al., 2021).

Zirconolites have been preferred among ceramic waste forms due to their efficiency in aqueous stability, chemical malleability, waste packing, and radiation hardness (Ma *et al.,* 2018; Shuaibu *et al.,* 2020). It has a stoichiometry of $CaZr_xTi_{3-x}O_7$ for $0.85 \leq x \leq 1.30$ in a monoclinic crystal structure (zirconolite-2M) with a *C2/c* space group (Blackburn *et al.,* 2020). In addition, Zirconolite revealed various polytypes properties related to stacking order among CaO_8/ZrO_7 polyhedra and TiO_6 due to lanthanide/actinide integration and fractional oxygen pressure as reported (Wei *et al.,* 2021). Experimentally, various oxidation states and ionic radii of actinides and lanthanides have been potentially doped within zirconolite-2M through substitution schemes consisting of direct and charge-compensated substitutions (Jafar *et al.*, 2014). The lanthanide/actinide ions with a valency of 3+ or 4+ might directly replace Ca, Zr, and/or Ti sites in direct substitution. For charge-compensated substitution, Ca and/or Zr sites may be replaced by the lanthanides or actinides after substituting Ti sites with a charge-compensated ion to neutralize the charges (Loiseau *et al.,* 2003; Whittle *et al.*, 2012). Many literatures have presented studies on the charge-compensated substitution mechanism in the zirconolite-2M phase. The charge-compensated ions comprise Cs, Mg^{2+}, Al^{3+}, Fe^{3+}, and Nb^{5+} (Lago *et al.,* 2022; Ma *et al.,* 2018; Zhou *et al.*, 2022).

Interestingly, the properties of a material can be improved by doping, that is, the introduction of impurities within a chemical structure to tune the properties of the material. The doping strategy has been widely reported to potentially alter materials' physical and chemical properties (Haruna *et al.*, 2020; Ilie *et al.,* 2018). Tanti and Kaltsoyannis (2021) investigated the effects of doping actinides and Ce into Zirconolite employing periodic DFT and molecular dynamics simulation (MD). The results indicated a redox behaviour and solid correlations between the ions' substitutional energies, a ratio of substituents ionic radius, and substituted ions.

The incorporation of trivalent at the Ti site has been investigated widely, indicating phase evolution and solubility of lanthanide/actinides in zirconolites (Zhou et al., 2022). However, no effect of divalent such as Mg^{2+} incorporation at the Ti site regarding phase evolution and lanthanide/actinides solubility was investigated. Magnesium (Mg) has been widely known as the natural constituent of zirconolite mineral and spent nuclear fuel (Barlow et al., 2021; Zhou et al., 2022). The Mg incorporation into Zirconolite would affect radionuclides' solubility limits and substitution mechanism. To the best of our knowledge, this is the first first-principle investigation to highlight Mg incorporation into Zirconolite.

COMPUTATIONAL DETAILS

The computations are conducted on the $2 \times 2 \times 2$ supercells comparative to the standard primitive unit cell of Magnesium doped Zirconolite $CaZrTi_2O_7$ within ab-initio calculation using Quantum ESPRESSO simulation package (QE) (Lawal *et al.,* 2018). Electron-electron interactions were treated using Perdew-Burke-Ernzerhof's generalized gradient approximation (PBE-GGA) (Perdew *et al.,* 1996). Integrals were evaluated using Maxfessel-Paxton's smearing method. $6 \times 6 \times 6$ k-points grids for all the materials and $50\ Ry$ has been chosen for the kinetic energy cut-off based on the Monkhorst-Pack scheme for the Brillouin zone integration. Also, XCrysden (X-window Crystallin Structure and Densities) a program for visualization for electronic and structural analysis, was applied (Shuaibu et al., 2021). The supercells relative to the primitive unit cell were applied, consisting of forty-four atoms: four Calcium atoms, four Zirconium atoms, eight Titanium atoms, and twenty-eight Oxygen atoms. One Titanium (Ti) atom was substituted by a Magnesium atom, giving $12.5\ \%$ possession by the dopant. The supercell dimensions were maintained for the whole calculations, while the atomic positions were relaxed for all calculations using Broyden-Fletcher-Golfarb-Shannon (BFGS) algorithm, till the acting forces on the atoms reduced to $0.001\ eV/Å$.

RESULTS AND DISCUSSION

1.1 Convergence Test Results of Magnesium-doped $CaZrTi_2O_7$

Principal computations are computed based on convergence tests as a main requirement for DFT calculations (Shuaibu et al., 2020). Figure 1 shows the convergence results of Mg-doped Zirconolite, indicating variation of the total energy (E_{tot} (Ry)) with respect to (E_{cut} (Ry)). The Figure shows a sharp decrease in total energy as cut-off energy increases. However, the two measure turning points at E_{cut} of 30 and 40 Ry respectively. Furthermore, the total energy remains almost constant between E_{cut} of 50 and 70 Ry. Therefore, 50 Ry is considered as an optimized kinetic energy cut-off for Mg-doped Zirconolite.

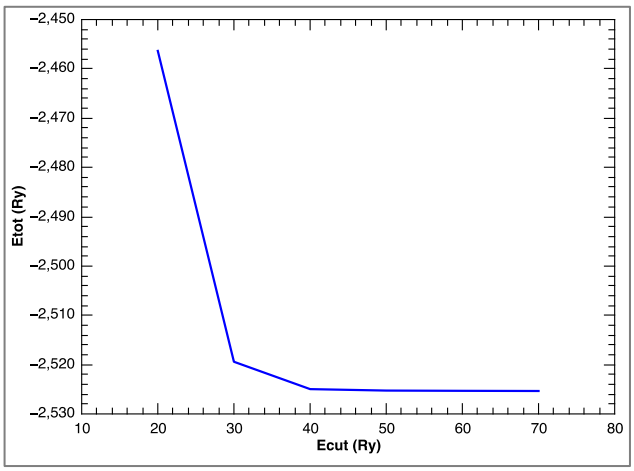

Figure 1. The convergence of total energy with respect to the kinetic energy cut-off.

Figure 2 shows the variation of total energy (E_{tot} (Ry)) versus the k-points mesh. The E_{tot} reduces significantly as the k-points mesh increases from $2 \times 2 \times 2$ to $6 \times 6 \times 6$. However, the E_{tot} was maintained from $6 \times 6 \times 6$ to $12 \times 12 \times 12$. Therefore, $6 \times 6 \times 6$ is considered an optimized k-point for Mg-doped Zirconolite (Appendix A; Table A1).

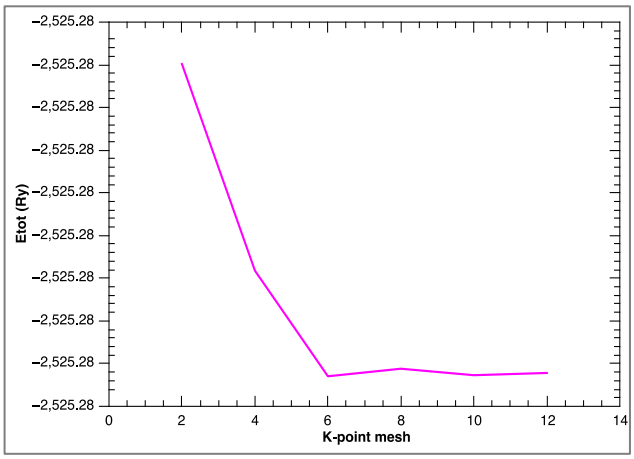

Figure 2. The convergence of the total energy with respect to the k-points grids.

1.2 Structural properties of Magnesium-doped $CaZrTi_2O_7$

Zirconolite structure with a space group *PI* showed triclinic geometry with high symmetry from which eight oxygen atoms are bonded to each Ti atom. It can be observed from Table 1 that eight various symmetrical approaches exist for $12.5\,\%$ of substitutional doping cases. In each case, Ti atoms can be substituted by Mg atoms (Figure 3). However, the D_8_0.125 configuration was considered for this particular study, and no structural changes were observed. Hence, the crystal parameters stayed stable. To obtain the stability of the structure after doping, the dopant formation energy (substitution energy) of the Mg atom was computed using **(1)** (Shamsudeen *et al.,* 2019). The substitution energy means the energy required to insert one Mg atom with a chemical potential μ_{Mg} into the supercell after removing one of the Ti atoms with chemical potential μ_{Ti} from the same position (Hanaor et al., 2012).

$$E_s = E_{doped} - E_{undoped} + \mu_{Ti} - \mu_{Mg} \qquad (1)$$

Where, E_{doped} is the total energy of the Mg-doped zirconolite $CaZrTi_2O_7$ material; $E_{undoped}$ is the total energy of the total energy of the undoped Zirconolite $CaZrTi_2O_7$ system; μ_{Ti} is the chemical potential per atom of Ti bulk crystal; μ_{Mg} is the chemical potential per atom of Mg bulk crystal. The chemical potential was numerically computed as the DFT total energy per atom in the bulk systems (Shamsudeen *et al.*, 2019). The dopant substitution energy of the $CaZrTi_2O_7$-Mg was determined a $1.424\ eV$ (from **Table 2**) and it evaluates the degree of stability of the doped structure. The lesser the substitution energy, the greater the stability of a structure. Therefore, the Mg-doped $CaZrTi_2O_7$ has demonstrated a stable structure based on the calculated value of the substitution energy.

Table 1: Configurations for substitutional doping of Ti by Mg zirconolite $CaZrTi_2O_7$ material.

Undoped	Ti	Ti	Ti	Ti	Ti	Ti	Ti	Ti
D_1_0.125	Mg	Ti	Ti	Ti	Ti	Ti	Ti	Ti
D_2_0.125	Ti	Mg	Ti	Ti	Ti	Ti	Ti	Ti
D_3_0.125	Ti	Ti	Mg	Ti	Ti	Ti	Ti	Ti
D_4_0.125	Ti	Ti	Ti	Mg	Ti	Ti	Ti	Ti
D_5_0.125	Ti	Ti	Ti	Ti	Mg	Ti	Ti	Ti
D_6_0.125	Ti	Ti	Ti	Ti	Ti	Mg	Ti	Ti
D_7_0.125	Ti	Ti	Ti	Ti	Ti	Ti	Mg	Ti
D_8_0.125	**Ti**	**Ti**	**Ti**	**Ti**	**Ti**	**Ti**	**Ti**	**Mg**

Table 2: Calculated total and Fermi energy of pure and Mg-doped *$CaZrTi_2O_7$*

Material	Total energy (Ry)	Fermi energy (eV)
Pure *$CaZrTi_2O_7$*	-2569.44129866 (Shuaibu *et al.*, 2020)	9.6918 (Shuaibu *et al.*, 2020)
Mg-doped *$CaZrTi_2O_7$*	-2525.27914843	42.9868 (This work)

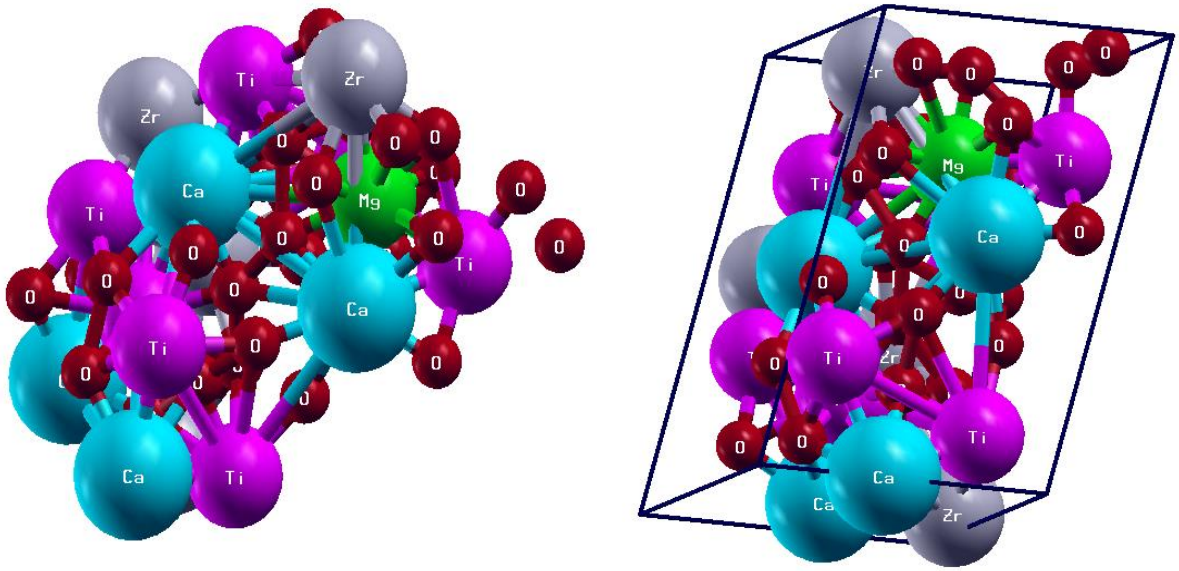

Figure 3. The bulk structure of simulated Mg-doped Zirconolite: red (small dark) spheres show oxygen ions, grey (large grey) spheres show zirconium ions, cyan (large cyan) spheres show Calcium ions, and purple (large purple) spheres show Ti ions, green (large green) show Magnesium.

3.2 Electronic Properties of Magnesium-Doped Zirconolite

The determination of the electronic properties of a material is important to allow the interpretation of the solid's properties (Lawal *et al.,* 2018; Radzwan *et al.*, 2020). The investigation of electronic properties of Mg-doped Zirconolite comprises the electronic band structure, density of state (DOS), partial density of state (PDOS), and charge density distribution. Mg was added to pure $CaZrTi_2O_7$ in the calculations targeting the *Ti* side to understand the effects of doping. Each Mg atom substitutes one of the *Ti* atoms on the $CaZrTi_2O_7$ perfect crystal plane, and the Mg atom is joined with the *Ti* atoms to make *Ti-Mg* bonds. The calculated electronic band structures of Mg-doped $CaZrTi_2O_7$ are shown along the eleven symmetry $(\Gamma\text{–}X\ |Y\text{–}\Gamma\text{–}Z\ |\ R_2\text{–}\Gamma\text{–}T_2\ |\ U_2\text{–}\Gamma\text{–}V_2)$ directions, and the energy of band structure separation is plotted from $-2.0\ eV$ to $2.0\ eV$ (Figure 4). The Fermi level is the zero-energy scale on the band structure. A generalized gradient approximation (PBE-GGA) was preferred over Local Density Approximations (LDA) due to its reliability and accuracy in DFT calculations. The energy partition between the CBm and the VBm occurred at R_2 and Γ points, respectively, indicating an indirect band gap material with a 0.06 eV energy gap. The energy band gap revealed its semiconductor behaviour. It is worth noting that the energy band gap reduces considerably with the undoped simulated Zirconolite found at 2.90 eV as shown in Figure 4.

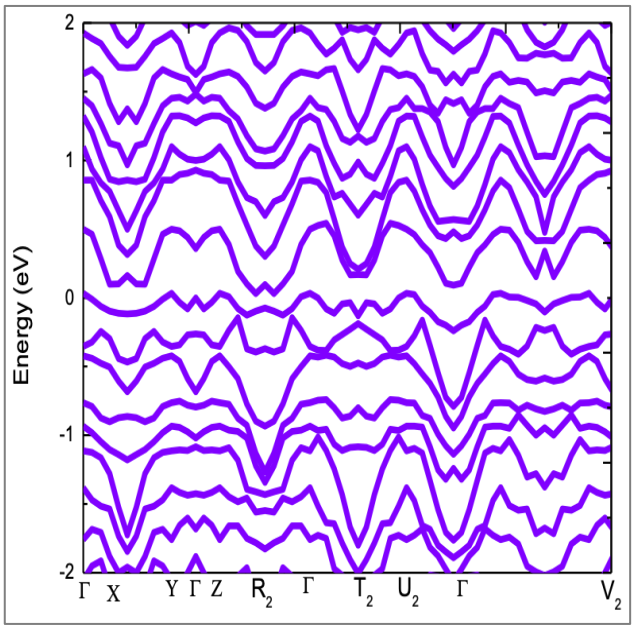

Figure 4. Calculated band structure of Magnesium (Mg) doped Zirconolite ($CaZrTi_2O_7$) compound.

Total DOS and PDOS were studied to understand clearly the nature of the energy gap. DOS describes the number of states per each energy level available for occupation and the nature of the band gap, and PDOS explains the origin of the valence and conduction band (Shuaibu et al., 2021). Figure 5 shows the DOS and PDOS results, respectively. Both figures illustrate the presence of higher and lower peaks at the conduction band and the valence band. The lowest valence states are dominated by *Ca-3s, Zr-4s, Ti-3s, Mg-2s-2p,* and *O-2s* orbitals which occurred approximately within (0.0 eV to -4.0 eV). The *Ca-3s, Zr-4s Ti-3s, Mg-2p,*

and *O-2p* orbitals highly contributed in the conduction band for *Mg*-doped $CaZrTi_2O_7$ (0.0 eV to 4.0 eV). The major contribution of the valence band close to the Fermi level is from *Ca-3p, Zr-4p, Ti-3p, and O-2p orbitals*. The greater contribution was observed from *Zr-4d* and *Ti-3d* orbitals near the Fermi level. Therefore, these materials might have been responsible for the change in the material's properties.

Table 3. The calculated energy gap of $CaZrTi_2O_7$ and *Mg*-doped $CaZrTi_2O_7$ with previous first principle calculations and experimental data.

Material	Method	Bandgap E(eV)	Nature	Reference
Pure $CaZrTi_2O_7$	Experimental	3.60	Indirect	(Mulroue, 2013)
Pure $CaZrTi_2O_7$	Computational	2.90	Indirect	(Shuaibu *et al*, 2020)
Mg-doped $CaZrTi_2O_7$	Computational	0.06	Indirect	This work

The charge density distribution has been plotted to understand the chemical bonding made by the atoms. The charge density distribution along the cations (Ca^{2+}, Zr^{4+}, Ti^{4+}, and Mg^{2+}) are spherical, indicating charge transfer between the atoms, as shown in Figure 6. The plots indicate ionic bonding formed by the ions. The thermometry scale from the Figure shows that the magenta color has the highest charge (+7.4369), which relates to the maximum charge accumulation of titanium atoms. However, the magnesium atom has a lower charge density (+0.1976). This indicates that titanium has the greatest charge density distribution in comparison to the remaining atoms.

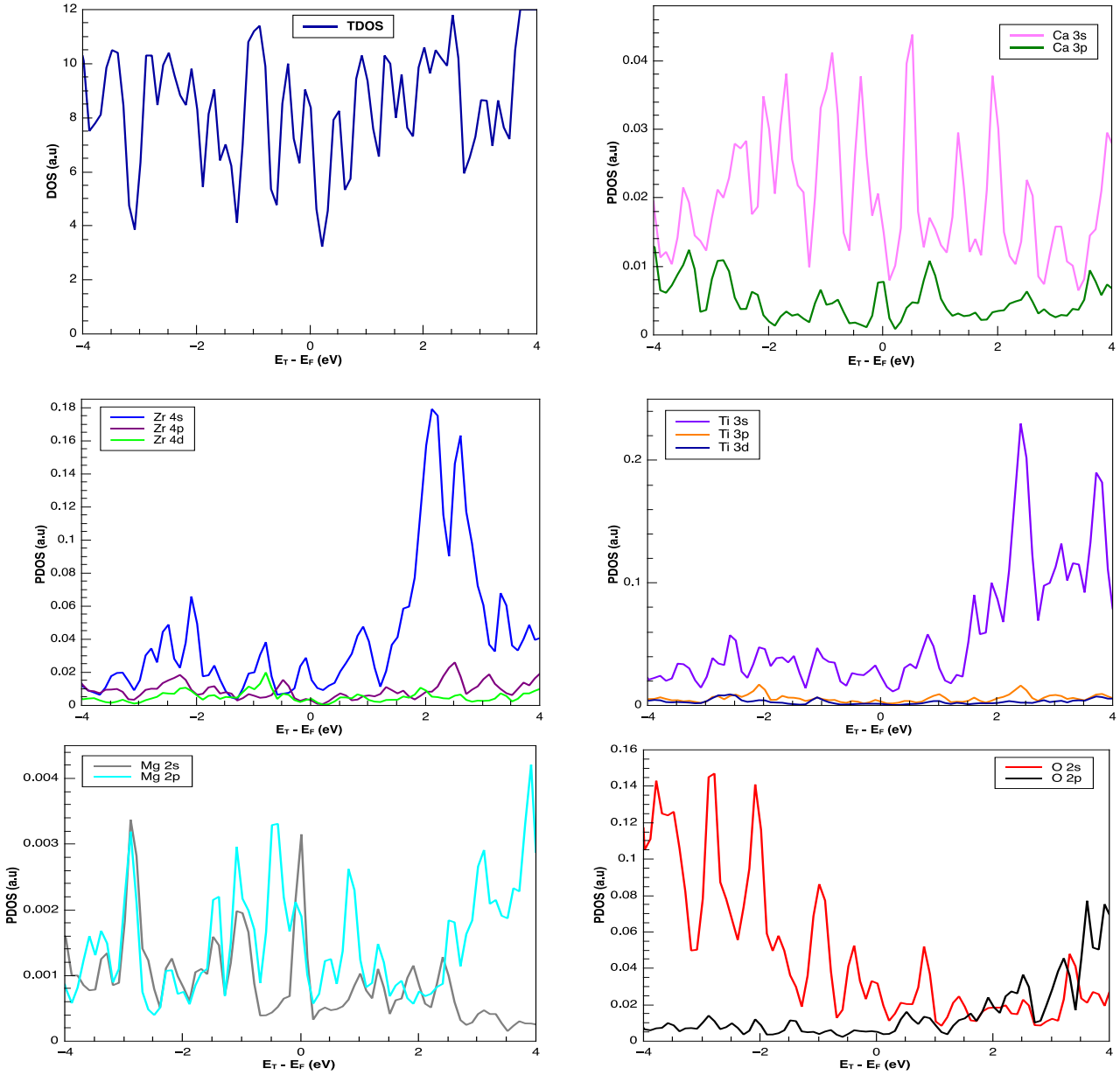

Figure 5. The total density of states and the partial density of states of Mg doped $CaZrTi_2O_7$.

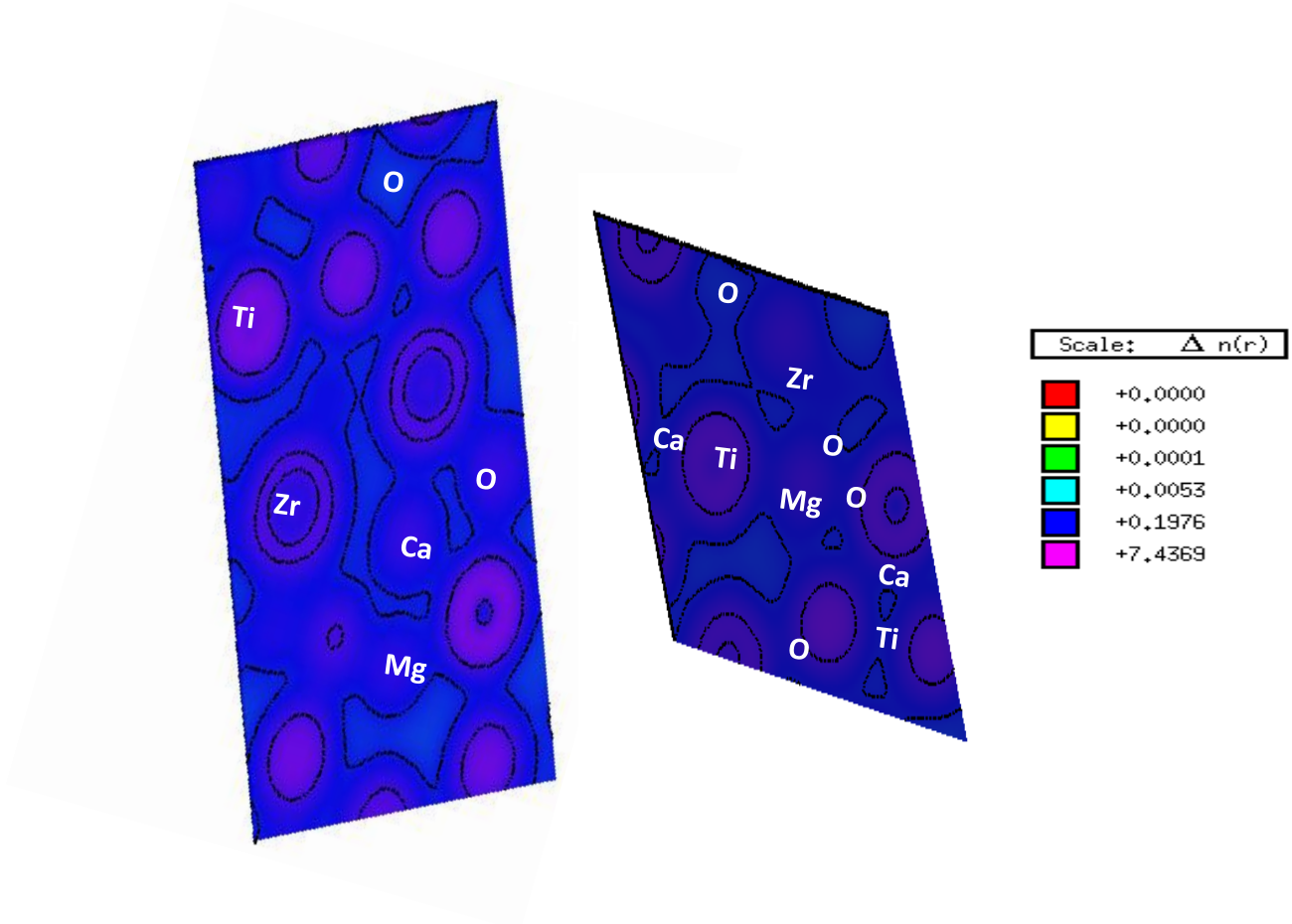

Figure 6. The charge density plot for the Magnesium (Mg) doped Zirconolite ($CaZrTi_2O_7$) in different planes. The scale n(r) indicating ranges of isodensity values in atomic unit (a.u).

CONCLUSION

The structural stability and electronic properties of Magnesium (Mg) doped Zirconolite (*$CaZrTi_2O_7$*), which is the potential ceramic for Radioactive High-Level Waste immobilization, have been investigated using Quantum ESPRESSO Code within Density Functional Theory (DFT). A generalized gradient approximation (PBE-GGA) was used for total energy calculation. The Mg-doped *$CaZrTi_2O_7$* was confirmed based on an effective crystal plane model. A Mg atom substituted one of the Ti atoms on the surface of the zirconolite *$CaZrTi_2O_7$* crystal plane. The dopant substitution energy of Magnesium is computed to be $1.424\ eV$. The substitution energy acts as the degree of stability of the doped structure. The lower the substitution energy, the higher the stability of the structure. Based on the value obtained, Magnesium doped zirconolite *$CaZrTi_2O_7$* appears to be a stable structure. The electronic properties such as density of state (DOS), the partial density of state (PDOS), and band gap value of Mg-doped *$CaZrTi_2O_7$* were computed. The results reveal an indirect band gap energy of 0.06 eV which indicated its metallic behaviour. This band gap energy under-estimation is due to the DFT approach limitation based on applied exchange-correlation functional. The findings indicate proper accommodation of Mg into Zirconolite which could enhanced an incorporation of actinides/lanthanides into zirconolite structure. However, The Mg-doped Zirconolite could be investigated further for defect stability, vibrational stability and thermal properties.

DECLARATION OF COMPETING INTEREST

The author declares no competing financial or personal interest to affect the work reported in this work.

REFERENCES

Aliyu, Y., Ibrahim, N., Yahaya, B., & Muhammad, A. (2024). Ab-initio investigation of gadolinium zirconate pyrochlore for substantial nuclear waste applications. *A Periodical of the Faculty of Natural and Applied Sciences, UMYU, Katsina, 3(2),* 180–185. **[Crossref]**

Barlow, S. T., Fisher, A. J., Bailey, D. J., Blackburn, L. R., Stennett, M. C., Hand, R. J., Morgan, S. P., Hyatt, N. C., & Corkhill, C. L. (2021). Thermal treatment of nuclear fuel-containing Magnox sludge radioactive waste. *Journal of Nuclear Materials, 552,* 152965. **[Crossref]**

Blackburn, L. R., Bailey, D. J., Sun, S. K., Gardner, L. J., Stennett, M. C., Corkhill, C. L., & Hyatt, N. C. (2021). Review of zirconolite crystal chemistry

and aqueous durability. *Advances in Applied Ceramics, 120(2),* 69–83. **[Crossref]**

Blackburn, L. R., Sun, S. K., Lawson, S. M., Gardner, L. J., Ding, H., Corkhill, C. L., Maddrell, E. R., Stennett, M. C., & Hyatt, N. C. (2020). Synthesis and characterisation of Ca1-xCexZrTi2-2xCr2xO7: Analogue zirconolite wasteform for the immobilisation of stockpiled UK plutonium. *Journal of the European Ceramic Society, 40(15),* 5909–5919. **[Crossref]**

Hanaor, D. A. H., Assadi, M. H. N., Li, S., Yu, A., & Sorrell, C. C. (2012). Ab initio study of phase stability in doped TiO2. *Computational Mechanics, 50(2),* 185–194. **[Crossref]**

Haruna, A., Abdulkadir, I., & Idris, S. O. (2020). Photocatalytic activity and doping effects of BiFeO3 nanoparticles in model organic dyes. *Heliyon, 6(1).* Elsevier Ltd. **[Crossref]**

Hurley, D. H., El-Azab, A., Bryan, M. S., Cooper, M. W. D., Dennett, C. A., Gofryk, K., He, L., Khafizov, M., Lander, G. H., Manley, M. E., Mann, J. M., Marianetti, C. A., Rickert, K., Selim, F. A., Tonks, M. R., & Wharry, J. P. (2022). Thermal energy transport in oxide nuclear fuel. *Chemical Reviews, 122(3),* 3711–3762. **[Crossref]**

Ilie, A. G., Scarisoreanu, M., Dutu, E., Dumitrache, F., Banici, A. M., Fleaca, C. T., Vasile, E., & Mihailescu, I. (2018). Study of phase development and thermal stability in as-synthesized TiO2 nanoparticles by laser pyrolysis: Ethylene uptake and oxygen enrichment. *Applied Surface Science, 427,* 798–806. **[Crossref]**

Jafar, M., Phapale, S. B., Nigam, S., Achary, S. N., Mishra, R., Majumder, C., & Tyagi, A. K. (2021). Implication of aliovalent cation substitution on structural and thermodynamic stability of Gd2Ti2O7: Experimental and theoretical investigations. *Journal of Alloys and Compounds, 859,* 157781. **[Crossref]**

Jafar, M., Sengupta, P., Achary, S. N., & Tyagi, A. K. (2014). Phase evolution and microstructural studies in CaZrTi2O7 (zirconolite)-Sm2Ti2O7 (pyrochlore) system. *Journal of the European Ceramic Society, 34(16),* 4373–4381. **[Crossref]**

Lago, D. C., Sánchez, A. D., & Prado, M. O. (2022). Cesium immobilization in porous silica and ^{137}Cs self-heating simulations. *Journal of Nuclear Materials, 565.* **[Crossref]**

Lawal, A., Shaari, A., Ahmed, R., & Taura, L. S. (2018). Investigation of excitonic states effects on optoelectronic properties of Sb_2Se_3 crystal for broadband photo-detector by highly accurate first-principles approach. *Current Applied Physics, 18(5),* 567–575. **[Crossref]**

Loiseau, P., Caurant, D., Baffier, N., & Fillet, C. (2003). Structural characterization of polycrystalline (Nd,Al)-substituted zirconolite. *Materials Research Society Symposium - Proceedings, 757,* 243–250. **[Crossref]**

Ma, S., Ji, S., Liao, C., Liu, C., Shih, K., & He, W. (2018). Effects of ionic radius on phase evolution in Ln-Al co-doped $Ca_{1-x}Ln_xZrTi_{2-x}Al_xO_7$ (Ln = La, Nd, Gd, Ho, Yb) solid solutions. *Ceramics International, 44(13).* **[Crossref]**

Mathew, M. D. (2022). Nuclear energy: A pathway towards mitigation of global warming. *Progress in Nuclear Energy, 143.* **[Crossref]**

Mulroue, J. (2013). *Ab initio study of the effect of charge localisation on the properties of defects in magnesium oxide and zirconolite* (Doctoral dissertation, UCL [University College London]).

Musa, S. G., Aljunid Merican, Z. M., & Haruna, A. (2022). Investigation of isotherms and isosteric heat of adsorption for PW_{11}@HKUST-1 composite. *Journal of Solid State Chemistry.* **[Crossref]**

Neumeier, S., Arinicheva, Y., Ji, Y., Heuser, J. M., Kowalski, P. M., Kegler, P., Schlenz, H., Bosbach, D., & Deissmann, G. (2017). New insights into phosphate-based materials for the immobilisation of actinides. *Radiochimica Acta, 105(11),* 961–984. **[Crossref]**

Pastina, B., & Laverne, J. A. (2021). An alternative conceptual model for the spent nuclear fuel–water interaction in deep geologic disposal conditions. *Applied Sciences (Switzerland), 11(18).* **[Crossref]**

Perdew, J. P., Burke, K., & Ernzerhof, M. (1996). Generalized gradient approximation made simple. *Physical Review Letters, 77(18),* 3865–3868. **[Crossref]**

Radzwan, A., Ahmed, R., Shaari, A., & Lawal, A. (2020). First-principles study of electronic and optical properties of antimony sulphide thin film. *Optik, 202(October 2019).* **[Crossref]**

Schreinemachers, C., Leinders, G., Mennecart, T., Cachoir, C., Lemmens, K., Verwerft, M., Brandt, F., Deissmann, G., Modolo, G., & Bosbach, D. (2022). Caesium and iodine release from spent mixed oxide fuels under repository-relevant conditions: Initial leaching results. *MRS Advances, 7(5–6),* 100–104. **[Crossref]**

Shamsudeen, A., Shuaibu, A., Abdu, S. G., Abubakar, M. S., & Lawal, A. (2019). First-principles calculations of Fluorine-doped Titanium dioxide: A prospective material for solar cells application. *Journal of the Nigerian Society of Physical Sciences, 1(4),* 131–137. **[Crossref]**

Shuaibu, A., Abdu, S., Aliyu, Y., & Kauru, Y. A. (2020). An investigation of structural and electronic properties of zirconolite ($CaZrTi_2O_7$) using density functional theory. *FUW Trends in Science & Technology Journal, 5(3),* 943–947.

Shuaibu, A., Tanko, Y. A., Abdurrahman, Z., & Lawal, A. (2021). Effect of beryllium and magnesium doped stanene single layer on structural and electronic properties using density functional theory as implemented in Quantum ESPRESSO. *Computational Materials Science, 01(01),* 1–7.

Subba Rao, T., Panigrahi, S., & Velraj, P. (2022). Transport and disposal of radioactive wastes in nuclear industry. *Microbial Biodegradation and Bioremediation,* 419–440. **[Crossref]**

Tanti, J., & Kaltsoyannis, N. (2021). Computational study of the substitution of early actinides and Ce into zirconolite. *Journal of Nuclear Materials, 543,* 152525. **[Crossref]**

Wei, Z. J., Bao, W., Sun, S. K., Blackburn, L. R., Tan, S. H., Gardner, L. J., Guo, W. M., Xu, F., Hyatt, N. C., & Lin, H. T. (2021). Synthesis of zirconolite-2M ceramics for immobilisation of neptunium. *Ceramics International, 47(1),* 1047–1052. **[Crossref]**

Whittle, K. R., Hyatt, N. C., Smith, K. L., Margiolaki, I., Berry, F. J., Knight, K. S., & Lumpkin, G. R. (2012). Combined neutron and X-ray diffraction determination of disorder in doped zirconolite-2M. *American Mineralogist, 97(2–3),* 291–298. **[Crossref]**

Zhou, Y., Liao, C., Leung, K. M., Ma, S., Chan, T. S., & Shih, K. (2022). Low charge compensator (Mg^{2+}) causing a new REE-end 3O structure (REE = Rare Earth Element) and a different phase transformation in Nd^{3+} co-doped zirconolite: Investigation by X-ray structural analysis. *Ceramics International, 48(13),* 18596–18604. **[Crossref]**

APPENDIX A. SUPPLEMENTARY DATA

Convergence Test Results of Mg-doped Zirconolite

Table A1: Convergence test of Mg-doped $CaZrTi_2O_7$ based on total energy with respect to kinetic energy cut-off of the plane wave and total energy with respect to k-points grids.

S/N	Convergence test	Kinetic energy cut-off (Ry)	Total energy (Ry)
1		20	-2456.36208243
2	Mg-doped $CaZrTi_2O_7$ total energy	30	-2519.43384563
3	with respect to kinetic energy cut-off	40	-2524.98109508
4	of the plane wave.	50	-2525.27549136
5		60	-2525.32418651
6		70	-2525.35699485
		k-point mesh	**Total energy (Ry)**
1		$2 \times 2 \times 2$	-2525.27549136
2	*Total energy with respect to the k-points*	$4 \times 4 \times 4$	-2525.27791251
3	*grids of Mg-doped $CaZrTi_2O_7$.*	$6 \times 6 \times 6$	-2525.27914843
4		$8 \times 8 \times 8$	-2525.27905949
5		$10 \times 10 \times 10$	-2525.27913615
6		$12 \times 12 \times 12$	-2525.27910915